

Microwave combustion synthesis method to prepare indium tin oxide NPS for sensor

Abstract

Indium tin oxide was prepared by using Microwave synthesis technique and it was characterised by using X-ray diffractometers, UV-Vis spectrometer and photoluminescence spectrometer, the as prepared samples were directly annealed for 200°C and then characterised. Morphological studies were analysed by using Transmission Electron Microscopy and Selective area diffraction pattern. The crystal sizes were calculated and it ranges from 9 to 12nm. The band gap values were calculated and it ranges from 2.49 to 3.015eV. The photoluminescence emission started from 340nm and its excitation values were nearly its near band edge emission at 360nm.

Keywords: ITO, In₂O₃, SnO₂ and XRD

Volume 2 Issue 5 - 2018

R Perumalsamy,^{1,2} S Nivetha,^{1,5} P Ponsurya,³ BH Abbas Shahul Hameed,⁴ A Ayeshamariam^{1,5}

¹Research and Development Center, Bharathidasan University, India

²Department of Physics, Sir Thiyagaraya College Higher Secondary School, India

³Department of Mechanical Engineering, Loyola ICAM College of Engineering and Technology, India

⁴Department of Mechanical Engineering, SMR East Coast College of Engineering and Technology, India

^{1,5}Department of Physics, Khadir Mohideen College, India

Correspondence: A Ayeshamariam, Department of Physics, Khadir Mohideen College, India, Email aismna786@gmail.com

Received: June 19, 2017 | **Published:** November 29, 2018

Introduction

Nanometer sized particles have unusual mechanical, optical, magnetic and electrical properties that make them of interest for novel applications. There is no universally agreed definition of a nanoparticle, However most research groups consider that particles with at least one dimension smaller than 100nm are nanoparticles and those with dimension in the range $100\text{nm} < d < \sim 10\mu\text{m}$ are called microparticles. The physical properties of the nanoparticles can vary significantly as the particle size changes.¹ The specific properties of nanoparticles include² dispersability in an immiscible phase, uniformity and fine grain size, extremely high specific surface area, control of the scattering of light, enhanced chemical activity of atoms and molecules at the interface, absorptive capabilities, microstructure control, transport properties of small domains and in pores, controlled electronic states of atoms etc. Due to these properties, nanoparticles have numerous commercial and technological applications.³ For instance, because of their very small size (20 times smaller than the wavelength of the visible light), they do not scatter light providing new perspectives for optical coatings.⁴ Their large specific area make them attractive to realize chemical or physical sensors for detecting the state of chemical reactions.⁵ Also these nanoparticles demonstrate quantum effect resulting in material innovations in communication, data storage, non-linear optic or with special magnetic properties.⁶ Many of these applications deal with dispersions or coatings with enhanced specific features. Much of the demand comes from the cosmetic and pharmaceutical industries⁷ where they show incredible commercial potential as for example to shield the skin from particularly damaging ultraviolet irradiation.⁸ In the field of medicine, magnetic nanoparticles found application particularly for the precise delivery of drugs to the exact target tissue by application of external magnetic fields. Various methods were used for synthesizing nanoparticles. The first development was made by Gleiter and Siegel⁸ by evaporation and condensation (nucleation and growth). This method, called gas phase synthesis, is similar to the physical vapour deposition (PVD),

but instead of using a substrate, liquid nitrogen is used to condense the vaporized material. The disadvantages of this method are the high temperature processing, the difficulty to control the particle size and distribution and the low production rate. Various aerosol processing techniques have been then reported to improve the production yield of nanoparticles. These include synthesis by combustion flame, plasma, laser ablation, chemical vapor condensation, and plasma spray. The chemical synthesis of nanoparticles is a promising technique to produce nanomaterials via low temperature processes. The sol-gel process (discussed in the next section) can form nanoparticles starting with precursors of different composition and structure. The institute of new materials (INM) in Saarbrucken is one of the few research centers which succeeded to produce a broad range of nanoparticles like TiO₂, Al₂O₃, BaTiO₃, ITO, ATO, etc through this process. The new materials built with these nanoparticles have already found many industrial applications.

Transparent conducting oxides (TCO) are the most common used materials to produce transparent conducting films. They are essentially based on In₂O₃, SnO₂, ZnO, CdO, etc. These materials are usually insulators and have a wide band gap ($E_g > 3\text{eV}$), so that they show an excellent transparency in the visible region. To get them conducting nonstoichiometry and/or appropriate dopants, like Sn for In₂O₃, Sb, F for SnO₂, Al, Ga for ZnO, etc., should be introduced in order to create electron degeneracy in the wide band gap.⁶ The number of products and technologies that used these materials on a variety of substrates (glass, plastic, ceramic, metal, etc.) is growing tremendously. TCO thin films can now widely utilized for optoelectronic devices, such as flat panel displays, thin film transistors, electroluminescent devices, heat reflectors, gas sensors, organic light emitting diodes, solar cells and variety of other significant applications in demisting and deicing glass for automotive, train and aircraft (52-59).

A colloidal suspension, as defined it is a system consisting of two phases, i.e. a continuous phase in which the other phase, containing entities having at least on the 1 to 1000 nm length scale, is dispersed.

The particles in the suspension undergo a Brownian motion and collide with each other. When they come close enough to each other, they stuck due to the Van der Waals attraction and aggregates are formed leading to phase separation. The aggregation of particles can be prevented or reduced by different mechanisms. The steric force is a repulsive force used to prevent the particle to come close to each other by attaching physically or chemically a surfactant or polymers to the surface of the particle. When two particles with their envelopes of organic chains approach each other, the chains in the gap between the particles lose its conformational entropy and resist a further approach.⁹ This dispersion (or stabilization) repulsive force is a function of the surfactant coverage, the type of bond formed at the surface and the type of the solvent. The electric charging of the particle can arise from different mechanisms and can be manipulated and controlled by adjusting the suspension pH and by using suitable dispersants. This is done by measuring the so-called zeta potential. The electrical potential drops off exponentially with the distance from the particle and reaches a uniform value in the solvent outside the diffuse double layer. The zeta potential is the voltage difference between a plane at short distance from the particle surface and the solvent beyond the double layer when two particles come close together so that their double layers overlap, they repel each other. The strength of the electrostatic force depends on the zeta potential. If it is too small (typically less than about 25mV, the repulsive force is not strong enough to overcome the Van der Waals attraction between the particles and they start to agglomerate. A high zeta potential prevents the particle-particle agglomeration and keeps the dispersion uniform

and free flowing. Therefore, the goal in most formulations is to maximize the zeta potential. This is particularly important to produce high strength ceramic materials.¹⁰

Experimental

ITO powder samples were prepared by simple combustion method. (90wt %) 10.033g of Indium metal and was dissolved with HNO_3 and equal amount of water is used to dilute the solution. Once in 3 hours it was warmed for about 48 hours, Indium metal dissolved in the solution. (10wt %) 1.2g of Sn metal was dissolved in the mixture of 5ml of HNO_3 and 45ml of H_2O . Now the reaction solution was taken by mixing 0.9ml of $\text{In}(\text{NO}_3)_3$ and 0.1ml $\text{Sn}(\text{NO}_3)_2$ with 10ml of water. 0.1 molar solution 0.5g of Urea ($\text{CONH}_2)_2$ was mixed with this mixture. This urea acting as a redox condensing agent used to precipitate ITO nano-particles. The mixture was heated at 300°C in open air for $\frac{1}{2}$ hour. Like that the same procedure was repeated for the different compositions 0.85ml of $\text{In}(\text{NO}_3)_3$ and 0.15ml $\text{Sn}(\text{NO}_3)_2$ with 10ml of water, 0.80ml of $\text{In}(\text{NO}_3)_3$ and 0.20ml $\text{Sn}(\text{NO}_3)_2$ with 10 ml of water. Microwave synthesis was adopted because of very fast nucleation process, conventional process requires multiple steps and takes long time also this process was used to produce uniformed heating, fast thermal induction, homogeneous nucleating sites. The resultant mixtures of ITO particles for different compositions were characterized by XRD. In that ITO compound was confirmed.¹¹ The powder is then characterized to determine the phase structure and the crystallite size using XRD technique. The density and the specific (BET) surface area were also determined Figure 1.¹²



Figure 1 Experimental set up of ITO NPs at different proportions.

Oxygen valency urea calculation In_2O_3 90% SnO_2 10%

Formula $\text{CO}(\text{NH}_2)_2$ oxidation valency from periodic table

$$\text{H} = (+1) \times 4 = +4$$

$$\text{N} = (0) \times 2 = 0$$

$$\text{C} = (+4) \times 1 = +4 \quad = +6$$

$$\text{O} = (-2) \times 1 = -2$$



$$\text{Sn} = (+4) \times 1 = +4$$

$$\text{N} = (0) \times 2 = 0 = -8$$

$$\text{O} = (-2) \times 6 = -12$$



$$\text{In} = (+3) \times 1 = +3$$

$$\text{N} = (0) \times 3 = 0 = -15$$

$$\text{O} = (-2) \times 9 = -18$$

$$1 \text{ Sn}(\text{NO}_3)_2 + 9 \text{ In}(\text{NO}_3)_3 + n (+6) = 0$$

$$1 (-8) + 9 (-15) + 6n = 0$$

$$-143 + 6n = 0$$

$$6n = 143$$

$$n = 23.833/100$$

$$n = 0.24\text{gm}$$

$$\text{Two times} = 0.48\text{gm}$$

$$0.48 \times 1.5 = 0.72\text{gm}$$

$$0.48 \times 2 = 0.96\text{gm}$$

The powder particles were pasted on the glass plates to find the diffusion and uniform distribution of the powder. In many reported

work for very small particles, surface area is a more appropriate characteristics to assess than some size based on an equivalent diameter. Particle surface area is important, for example, in paints and pigments or when chemical reactivity is an important property, as in the setting of cement. Precipitated materials are often characterized in this manner. Amongst the several techniques available, those based on permeability and gas adsorption are probably the most popular. In the permeability methods a known quantity of air is forced through a small bed of the fine solids under a constant pressure drop, and the flow time is recorded. The theory is based on the laminar flow of fluids through porous beds, and the specific surface area of the material is calculated from Kozeny equation (Figure 2).¹³

$$S^2 = \left(\frac{\Delta P}{k\eta L\rho^2} \right) \left(\frac{\varepsilon^3}{(1-\varepsilon)^2} \right) \quad (1)$$

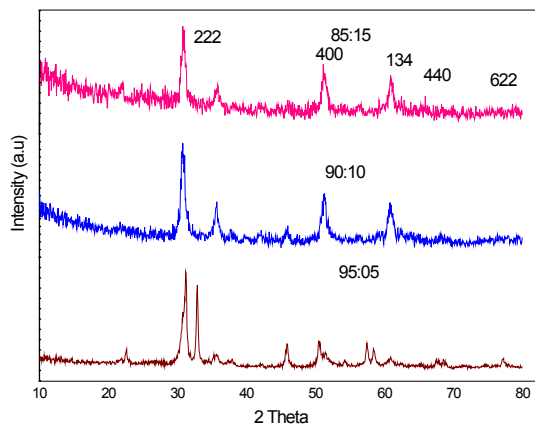


Figure 2 XRD diffraction pattern of ITO powder for three different proportions.

In the IT sectors, nano-particles are used for increasing the efficiency of electronic equipments by increasing the information storage capacity and decreasing the size and weight of the devices. While several synthesis and processing methods have been employed for making thin-films of ITO research on nano-particles, chemical methods is the best technique to synthesize ITO powdered nano-particles. Nano-particles are produced by various techniques, crystallization, precipitation, sol-gel methods, combustion and chemical vapour deposition methods.¹⁴ ITO nano-particles are synthesized here, by combustion method and its structures are characterized with XRD (X-ray Diffraction) (Figure 3–8).

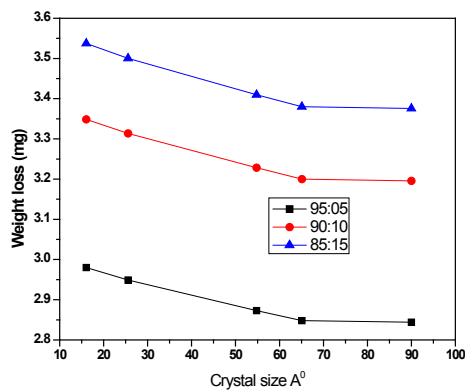


Figure 3 TGA analysis for different proportion of ITO nano powdered particle.

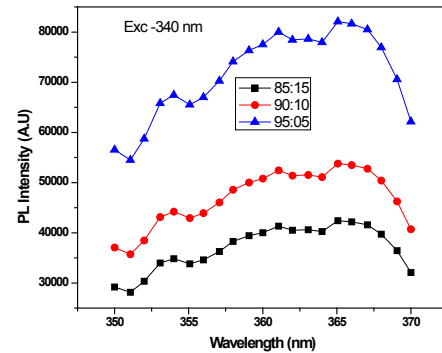


Figure 4 Photoluminescence values of ITO nanopowder.

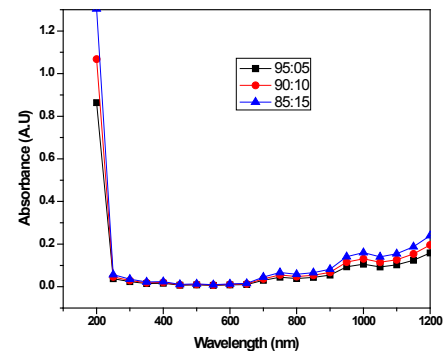


Figure 5 Photoluminescence values of ITO nanopowder.

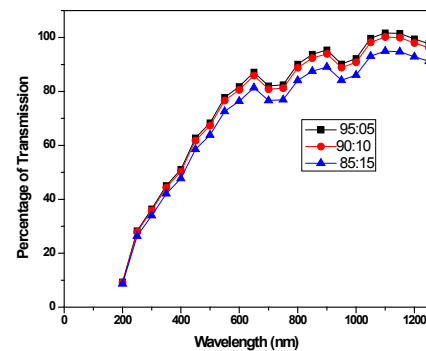


Figure 6 Percentage of transmission of ITO powder for different proportions.

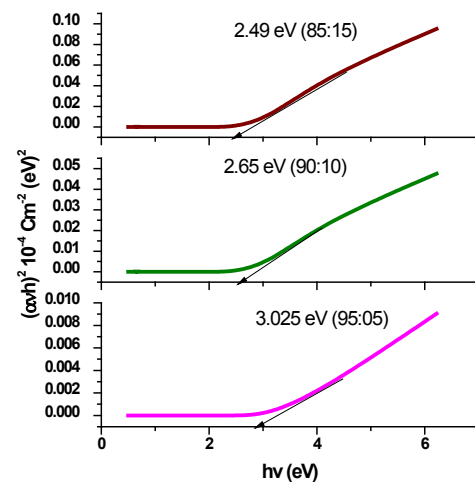


Figure 7 Bandgap values of ITO powder for different proportions.

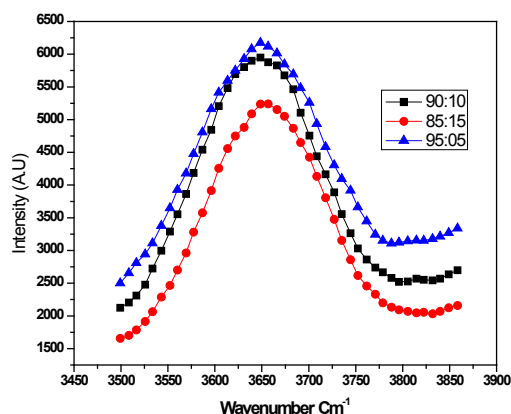


Figure 8 Raman analysis of ITO nanopowder.

Results and discussion

The X-Ray powder diffraction patterns were recorded using Panalytical X³pert Pro X-ray Diffractometer having wavelength $\lambda=1.5406\text{\AA}$. X-Ray Diffraction (XRD) is a high-tech, non-destructive technique for analyzing a wide range of materials, including fluids, metals, minerals, polymers, catalysts, plastics, pharmaceuticals, thin-film coatings, nano-particles, ceramics and semiconductors. The X-Ray Diffraction peaks could be indexed to ITO with cubic structure having lattice constant of $A=10.0259\text{\AA}$. The growth of small

dimension ITO peaks has been reported¹⁵ for different compositions. Studies of such structures are of interest because sharp tips are having same lattice planes [2,2,2.] This is useful for efficient field emission¹⁶ having potential applications in displays. The growth of peak morphology is ascribed to preferential adsorption of ITO species on some special crystallographic planes of Indium Tin Oxide. The grain size of the nano-crystalline powder is estimated by using Scherer formula

$$D = \frac{0.94\lambda}{\beta \cos \theta} \tag{2}$$

Where β full width half maximum of XRD pattern. The value of grain size varies from 9nm to 12nm for the different compositions. No. of unit cells for the ITO nano-particles was calculated by

$$n = \frac{4}{3} \pi \left(\frac{D}{2} \right)^3 \frac{1}{V} \tag{3}$$

where V is the volume of the cubic structure of ITO

$$V=a^3 \text{ \AA}^3 \tag{4}$$

$$\text{Lattice parameter } a = d\sqrt{h^2 + k^2 + l^2} \text{ \AA}, \tag{5}$$

No. of unit cells decrease when Indium composition decreases Figure 9a & Figure 9b.

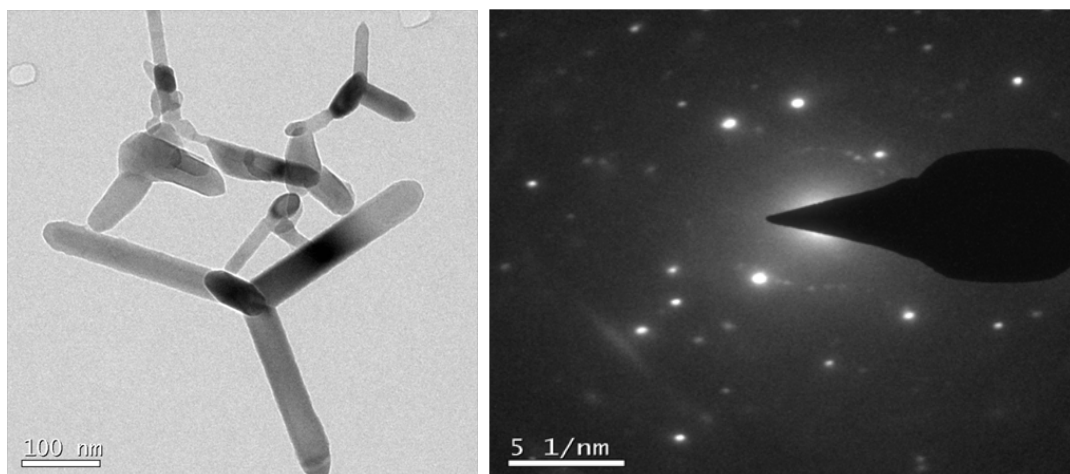


Figure 9a & Figure 9b TEM and SAED micrograph for 95:05 ITO nanopowder.

Studies of such structures are of interest because sharp tips are useful for efficient field emission¹⁰ having potential applications in displays. The presence of SnO_2 in In_2O_3 compound is indexed on the basis of JCPDS Card No-89 – 4596. For all proportion it is clear from the XRD spectra that the entire powder specimen are cubic structure and highly oriented along (222) plane. Presence of other orientations (400), (440), (622) and (134) have also been detected. The lattice parameters calculated from the most prominent peaks are found to be in agreement with JCPDS values listed in Table 1 & Table 2.

Table 1 Structural properties of ITO nanopowder

Samples	Grain Size (nm)	Lattice parameter (a)Å	Volume (m ³)	No.of.Unit cells (m)	Surface area from eqn 1 Sq/m ²	Urea	Bandgap
(85:15)	12.673	9.9646	989.42	1075.7	123	0.48	2.49
(90:10)	10.478	10.064	1019.36	525.6	156	0.72	2.65
(95:05)	9.0435	10.0491	1014.8	381.422	164	0.84	3.025

Explained the results of Percentage of Phase formation = $I_{\text{ITO}} / I_{\text{ITO}} + I_{\text{I}_0}$

I_{ITO} = Maximum intensity of ITO peak

I_{I_0} = Maximum Intensity of I_0 peak

I_{T_0} = Maximum Intensity of T_0 peak

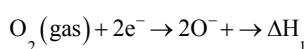
X ray Peak heights of ITO powder with random grain orientations.¹⁷

Table 2 Peak intensity and prominent peak positions of ITO nanopowder

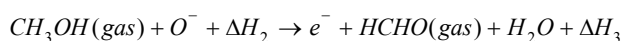
95:05:00	222	400	134	440	622
Ip	100	10.4	28.14	22.38	7.48
2q	31.0652	35.5328	45.8127	50.5498	60.7718
90:10:00	222	400	134	440	622
Ip	100	28.62	11.89	44.62	27.63
2q	30.7498	35.6015	45.8472	51.175	60.7923
85:15:00	222	400	134	440	622
Ip	100	26.73	55.33	41.23	7.5
2q	30.7975	35.7166	51.1948	60.8723	60.7923

Figure shows the variation of the relative change in resistance of sensors $S = \left(\frac{R_{vac} - R_{gas}}{R_{gas}} \right)$ with operating temperature in the

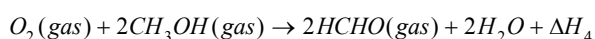
range 100°C-250°C. The sensitivities increase with the operating temperature (heater temperature) T_{op} , up to 200°C, but decreases after 200°C and it is found to be maximum at 200°C irrespective of the methanol concentration used. This temperature sensitive phenomenon is attributed to overcome the dynamic energy of activation and reaches the maximum value of sensitivity which satisfies the sensitizing and detection equation¹⁸ given below. For sensing reaction, gas to be detected is adsorbed with contact on the surface of the ITO film to form the Schottky contact and the electrical resistance of the sensor is changed as per the following reaction,



Then during the detection reaction, participation of oxygen which can be in molecular (O_2) or in atomic (O^-) form takes place to reduce the resistance of the film and the corresponding reaction is



On combining these two reactions,



The liberated water condenses on the sensing element, which saturates the surface and affects the sensitivity. Hence, for lower temperature operation, the surface of the sensor does not get completely desorbed, which causes only smaller change in resistance.

As the temperature of the sensing element increases, hydroxyl group is desorbed and decrease in resistance is observed which in turn increases the sensitivity.¹⁹ At high temperatures, the depletion region created by the chemisorption of oxygen on the surface extends more deeply providing larger scope to more number of gaseous elements to be adsorbed thereby giving a better response. One more possibility of the partial incorporation of Sn^+ ions in In^{3+} sites changes the carrier concentration and the work function on the surface. This allows more gaseous elements of methanol on the surface, leading to an improvement in the output response and the selectivity.²⁰

Response of the sensor versus methanol concentration

Figure shows the variation in the sensitivity of the indium tin oxide sensor (90:10) proportion in the presence of methanol vapor of various concentrations. The concentration is varied from 200ppm to 1000ppm. As seen, with an increase in the methanol concentration, the sensitivity of the sensor varies in a linear manner and attains maximum at 1000ppm. The response seems to be quite linear for the methanol concentration variation in the range from 200ppm to 600ppm. The sensitivity saturates in higher concentrations (>600ppm), because the number of active surface states at the film surface is limited. The measured sensitivity at 200°C is estimated to be around 8 for 200ppm of methanol gas where as it increases to 23 for 1000ppm. At lower concentrations, the gas sensitivity increases steeply with increase of the gas concentration from 200 to 600 ppm, obeying the standard law of metal oxide semiconductor devices.²¹

$$R_{gas} = R_{air} (1 + K[CH_3OH])^{-m}$$

where, $[CH_3OH]$ is the concentration of methanol in ppm, 'K' is the sensitivity co-efficient of CH_3OH vapor and 'm' is the power law exponent. At higher concentration of methanol, the increase in the gas sensitivity values becomes more gradual.²²⁻²⁴ The mechanism of sensitivity increase may be explained as follows. With a fixed surface area for each sample, a lower gas concentration implies a lower coverage of gas molecule on the surface and hence lower surface reaction occurred. An increase in the gas concentration tries to raise the surface reaction due to large surface coverage. Further increase in the quantity of surface reactions will be gradual and slow when the saturation point on the coverage of molecules at the fixed surface area is reached. This leads to saturation levels at which the upper limit of detection can be determined.

This observed linearity of sensitivity in the lower concentration range of methanol is suited for the use of these ITO films prepared in this work in checking the concentration of methanol. These ITO films may be used in the fabrication of sensitive methanol gas sensors (Figure 10a & Figure 10b).

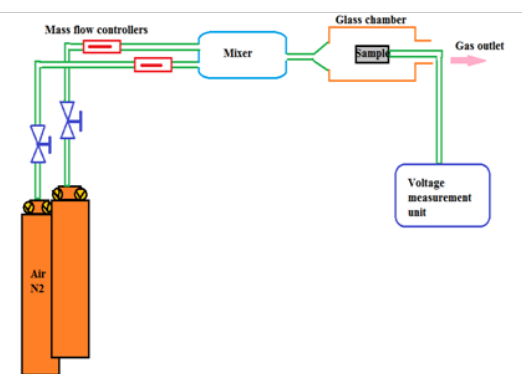


Figure 10a & Figure 10b Experimental set up of gas sensor at 95:05 ITO NPs the pellet thickness may be in 0.5 micro meter 5 mm diameter and contacted with aluminium dots or gold foils.

Sensor response and recovery times

The response and recovery times are important parameters based on which sensors for desired applications can be fabricated. The response time is defined as the time required for the sensitivity to reach 90% of the equilibrium value after the test gas is injected. The recovery time is the time necessary for the sensor to attain a sensitivity of 10% above the original value in air. The transient response curve of the ITO sensors are shown in Figure 11. The variation of the sensitivity was measured at an operating temperature of 200°C and methanol concentration of 1000ppm. Upon injection of methanol vapor, the sensitivity of ITO sensor reaches saturation in about 10 minutes.²⁴ When dry air was introduced, the sensitivity reached to the initial value. This fact proves the reversibility of the sensing process.

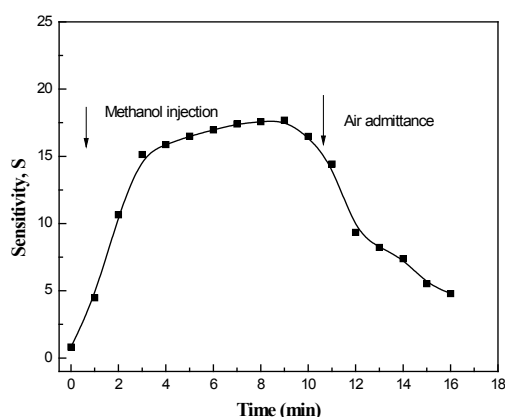


Figure 11 Transient response curve of the ITO methanol sensors for 95:05 proportions of ITO NPs.

Conclusion

The ITO (90:10) NPs were mounted by using two electrodes of Pt and rGO from ceramic target have been found to be sensitive to methanol vapor of varying concentrations. The characteristics of the ITO gas sensors were studied in an airtight chamber and are summarized as below. The relationship between sensitivity and concentration is found to be linear in the methanol concentration range from 200 to 600ppm. It reaches saturation in higher concentrations (>600ppm) and attains maximum at 1000ppm. The sensitivity increases with the operating temperature T_{op} , up to 200°C, but decreases after 200°C and found to be maximum at 200°C irrespective of the methanol concentration used. The sensor shows moderate response and recovery time (in minutes) (Figure 12 & Figure 13).

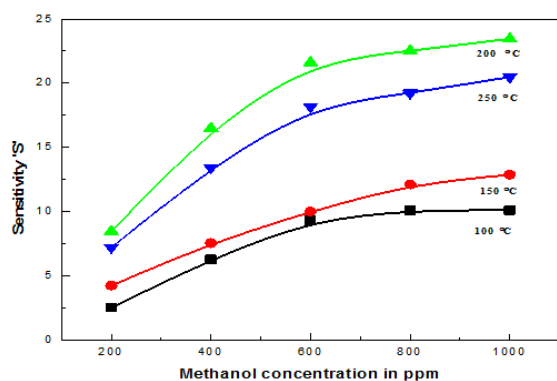


Figure 12 Variation of methanol concentration and sensitivity for the different substrate temperature of 95:05 ITO NPs.

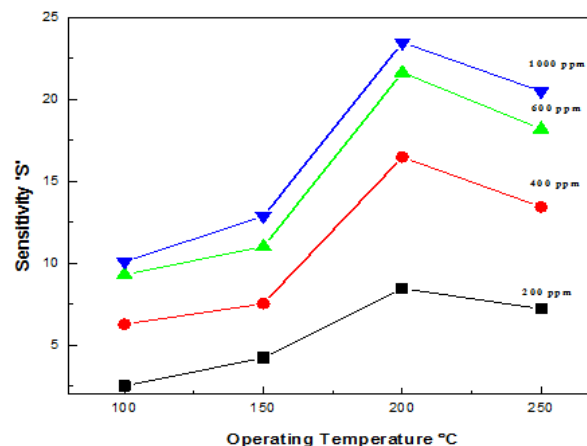


Figure 13 Variation of operating temperature and sensitivity of ITO 95:05 NPS at different ppm.

Acknowledgments

None.

Conflicts of interest

The author declares there is no conflicts of interest.

References

1. M Hines, P Guyot Sionnest. Synthesis and Characterization of Strongly Luminescing ZnS-Capped CdSe Nanocrystals. *J Phys Chem.* 1996;100(2):468–471.
2. H Weller. Colloidal Semiconductor Q-Particles: Chemistry in the Transition Region Between Solid State and Molecules. *Angew Chem.* 1993.
3. S Emory, S Nie. Screening and Enrichment of Metal Nanoparticles with Novel Optical Properties. *J Phys Chem B.* 1998;102(3):493–497.
4. A Haes, R Van Duyne. A Highly Sensitive and Selective Surface-Enhanced Nanobiosensor. *Mater Res Soc Symp.* 2002;723.
5. G Kataby, A Ulman, R Prozorov, et al. Coating of Amorphous Iron Nanoparticles by Long-Chain Alcohols. *Langmuir.* 1998;14(7):1512–1515.
6. Y Ohko, T Tatsuma, T Fujii, et al. Mechanisms of the Plasmon-Induced Charge Separation (PICS). *Journal of The Society of Photographic Science and Technology of Japan.* 2013;76(6):463–468.
7. J Kreuter. Drug targeting to the nervous system by Nanoparticles. *Medinova medical Consulting GmbH.* 1997.
8. D McRae, E Matijevec, EJ Davis. Chemical reactions in aerosols: II. The effects of various parameters on the bromination of 1-octadecene droplets. *J Colloidal Interface Sci.* 1978;67(3):526–537.
9. S Vemury, S Pratsinis. Corona-assisted flame synthesis of ultrafine titania particles. *Appl Phys Lett.* 1995;66(24).
10. Hideki yoshioka, Hiroshi Matsui, Muneyuki Motoyama. High-quality indium oxide films at low substrate temperature. *Appl Phys Lett.* 1999;74(20):3059–3060.
11. KG Gopchandran, B Joseph, JT Abraham, et al. The preparation of transparent electrically conducting indium oxide films by reactive vacuum evaporation. *Vacuum.* 1997;48(6):547–550.
12. M Schaepkens, GS Oehrlein. Effect of radio frequency bias power on SiO₂ feature etching in inductively coupled fluorocarbon plasmas. *Journal of Vacuum Science Technology.* 2000;18(2).

13. D Alina Magdas, Ana Cremades, Javier Piqueras. Growth and luminescence of elongated In_2O_3 micro- and nanostructures in thermally treated InN. *Applied Physics Letter*. 2006;88(11).
14. P Guha, S Kar, S Chaudhuri. Relevance of Microstructure on Optical Properties of Thermally Evaporated Indium Oxide Thin Films. *Open Access Library Journal*. 2015;2(1):1–15.
15. H Jia, Y Zhang, X Chen, et al. Electrochemically deposited zinc oxide arrays for field emission. *Applied Physics letter*. 2006;88(16).
16. Liquid Smoke. 2008.
17. Hideki yoshioka, Hiroshi Matsui, Muneyuki Motoyama, et al. High-quality indium oxide films at low substrate temperature. *Applied Physics Letters*. 1999;74(20).
18. Francis F Chen, Xicheng Jiang, John D Evans. Plasma injection with helicon sources. *Journal of Vacuum Science Technology*. 2000;18(5):2108.
19. G Rupprecht. Untersuchungen der elektrischen und lichtelektrischen Leitfähigkeit dünner Indiumoxydschichten. *Zeitschrift für Physik*. 1954;139(5):504–517.
20. RL Weiher, RP Ley. Optical Properties of Indium Oxide. *Journal of Applied Physics*. 1966;37(1):299.
21. BD Cullity. *Elements of X-ray diffraction*. 1978.
22. Guha P, Kar S, Chaudhuri S. Direct Synthesis of Single Crystalline In_2O_3 Nanopyramids and Nanocolumns and Their Photoluminescence Properties. *Applied Physics Letters*. 2004;85:3851–3853.
23. C X Xu, XW Sun. Electrochemically deposited zinc oxide arrays for field emission. *Applied Physics letter*. 2003;82:4146.
24. PS Devi, M Chatterjee, D Ganguli. Indium tin oxide nano-particles through an emulsion technique. *Materials Letters*. 2002;55(4):205–210.